XVI International Conference on Durability of Building Materials and Components
DBMC 2023, China
K.F. Li and D.P. Fang (Eds)

Application of Ultrasonic Computerized Tomography Technique to Detect the Internal Defects in Cement-based Mortar

Zhe Li[1], Kefei Li[1,]*, Junjie Wang[1] and Le Li[1]

[1]Department of Civil Engineering, Tsinghua University, Beijing 100084, PR China,
likefei@tsinghua.edu.cn

Abstract. *It is widely acknowledged that ultrasonic technology provides a considerable detection approach while describing the internal fractures in concrete, which is a serious issue when evaluating the durability performance of cement-based materials. This paper aims to introduce the work which is concerned with the use of ultrasonic computerized tomography (UCT) technique to evaluate the micro-cracks inside mortar. The result shows that UCT is a relatively promising method which is capable of imaging the positions of tiny cracks and local damage, moreover, the application of X-ray computerized tomography (XCT) also verifies the accuracy and reliability of UCT. Effective evaluating the internal cracks depends on the detection of attenuation of ultrasonic signals that perpendicular to internal cracks, furthermore, ultrasonic technology is more likely to detect the crack with larger surface of damage, but not sensitive to local fracture.*

Keywords: *Ultrasonic CT, Algorithm, Cracks, Durability, Mortar.*

1 Introduction

Cracking is one of the most serious issues when evaluating the durability performance of cement-based materials [1-3], which is concerned with the service life-span and also the reliability index of a building or construction [4, 5]. The cracks triggered by several impact factors such as reinforcements corrosion, shrinkage, creep, sulfate attack, et al., which may lead to a fatal damage to structural safety [6-8]. Hence, accurately describing the scale and trend of cracks in cement-based materials is the most significant composite of durability evaluation, especially for the internal cracks which cannot be observed by naked eyes [9, 10]. Ultrasonic testing is a practical technology that developing rapidly in recent years, and its basic principle is of a certain frequency excitation of the object to be tested in ultrasonic elastic wave, through the instrument by analyzing the signals, which will reveal the distributions of objects and the mechanics characteristics of the internal defects [11]. Ultrasonic detection has no damage to the measured object and the test is relatively simple, presently, which is widely applicated in many research fields [12].

The main principle of the ultrasonic method is by the difference of ultrasonic pulse velocity and transmission loss in different media. Ultrasonic wave propagates easily in dense medium, but diffraction or refraction will occur at the places of cracks, herein, the internal scales and directions of cracks can be detected and evaluated based on this mechanism. Recently, many researchers have reported their latest studies about ultrasonic computed tomography (UCT) technologies against cracks inside non-metallic material. Ham et al. [13] applicated contactless ultrasound toward automated inspection of concrete structures, both obtained surface wave velocity and attenuation signal characteristics show sensitivity to concrete material damage. Kim et al. [14] evaluated the drying shrinkage in concrete by nonlinear ultrasound (NLU), and

the results show that large changes in the measured acoustic nonlinearity parameter are attributed to the damage generated during drying shrinkage. Quiviger et al. [15] investigated the effect of the presence and size of a real macro-crack on diffuse ultrasound in concrete, which reveals the influence of the closed part of the cracks with regions in partial contacts on the diffusion parameters.

Even through ultrasound is a relatively reliable method and enormous researches have been carried out, there is still a huge gap to realize accurately describing the internal cracks inside concrete. Fortunately, the development of computerized tomography (CT) has provided an improved algorithm for imaging the formation of cracks of every single cross-section, based on the data collected by the ultrasonic device. In this paper, an improved algorithm will be proposed and combined with ultrasonic device, which aims to detect the internal cracks of cement-based materials.

2 Materials and Apparatus

2.1 Materials and Fabrication

P.I. 42.5 Portland cement was used as the binder materials and its chemical composites were shown as Table 1 (Chinese standard GB175-2007), and also, S95 GGBS (Chinese standard GB/T18046-2008) and Class I fly ash (Chinese standard GB1596-2005) were mixed as mineral admixtures and the chemical composites were also presented as Table 1. Table 2 shows the mix proportions of mortar and the water/binder ratio was set as 0.45, meanwhile, river sand with fineness modulus of 2.6 was used as fine aggregates. During the specimen fabrication process, fresh mortar was poured into the moulds (Fig.1), and then de-moulded after hardening and curing at 20±3 ℃ and 100% relative humidity for 28 days. After proper curing, the mortar specimens were suffered two types of damage, which includes a penetrating crack triggered by a concentrated at the side surface of cross section from a test machine, while another is a hole drilled by an electric hand drill and its diameter is in 12 mm (Fig.2).

Table 1 Chemical compositions of binder materials (w.t. %)

Constituent	SiO_2	Al_2O_3	Fe_2O_3	CaO	MgO	Na_2O	K_2O	SO_3	P_2O_5
Cement	21.98	4.79	3.29	64.60	2.05	0.56	0.48	2.09	0.12
GGBS	32.57	13.28	1.36	41.04	5.65	0.42	0.08	2.64	0.54
Fly ash	56.90	13.70	4.46	1.90	0.37	0.12	1.55	0.12	0.11

Table 2 Mix proportions of mortar (kg/m^3)

Cement	GGBS	Fly ash	Sand	Water	Super plasticizer
290	145	145	1250	260	3.5

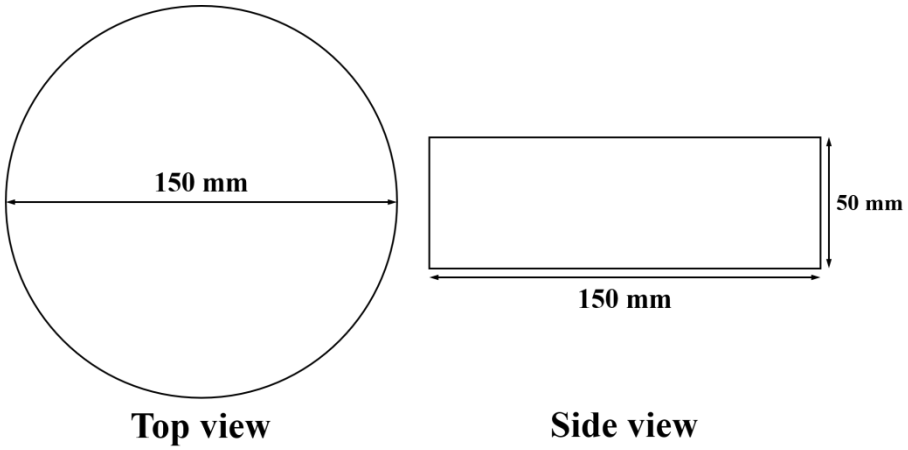

Fig.1 Schematic diagrams of the mould

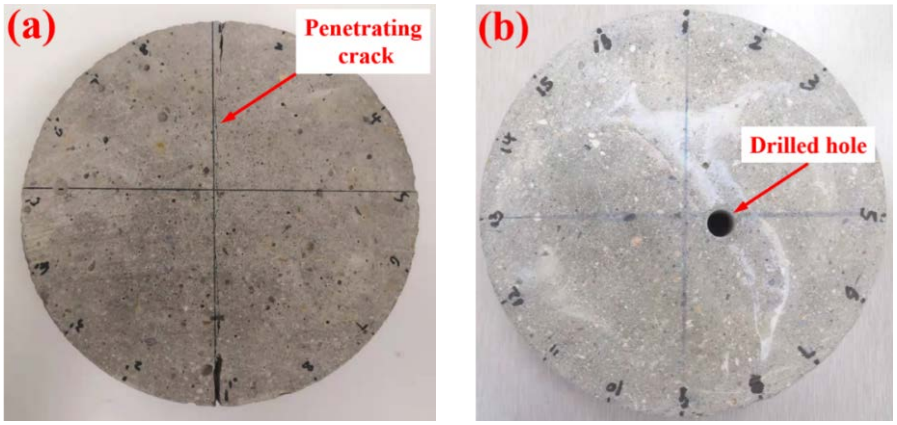

Fig.2 The mortar specimen with fabricated damage (a) With a penetrating crack (b) With a drilled hole

2.2 Ultrasonic Detection Apparatus

Nonmetallic ultrasonic detection is commonly used in low frequency (20-100 kHz) longitudinal wave probes. The ultrasonic detection apparatus used in this experiment was type Proceq PL-200 (from Switzerland, Fig.3) and a pair of ultrasonic probes with a frequency of 54 kHz, and its key parameters were shown in Table 3. As reported among published papers worldwide, 54 kHz is more suitable for detecting the internal defects of non-metallic materials, and also, the needle-nosed probes do not require coupling media. This device has the characteristics of baseline accuracy, high resolution, and is widely adopted worldwide. Type GE Vtomexs (from USA) X-ray detection apparatus was selected and its relevant key parameters were shown as Table 4, which is characterized by high energy resolution and is also capable of reflecting the locations and scale of cracks inside the mortar specimen accurately.

Fig.3 Type Proceq PL-200 ultrasonic apparatus

Table 3 Key parameters of ultrasonic apparatus (Type Proceq PL-200)

Frequency	Bandwidth	Driving voltage	Piezo electrical cell capacity	Contact surface diameter	Dimensions	Weight
54±5 kHz	＜10 kHz	From -1000 V to 1000 V	2 nF	4 mm	49.7 mm× 99.43 mm	244 g

Table 4 Key parameters of X-ray detection apparatus (Type GE Vtomexs)

Scanning voltage	Scanning current density	Exposure duration time	Accuracy	Power
220 kv	280 uA	1000 ms	1 μm	320 W

2.3 Mechanism of Improved CT Algorithm

The main principle of the ultrasonic CT technology is to use the strong reflection characters of ultrasonic wave on the interface of different media to reconstruct the media image, which can reflect the damage and fracture level of media. Because of the complexity of subsequent wave formation, the analysis of subsequent wave forms is relatively complicated, which is the reason that the acoustic duration time and amplitude of the first wave are the primary factors on ultrasonic detection. The specific operation steps of CT algorithm are as follows: first of all, the image reconstruction area is discretized into a number of numbered regular grid cells and regionalization operation is carried out in each cell, and then the regionalization operation result is iterated into the overall calculation result. Fig.4 shows the comparison of mesh generation between the traditional algorithm and the improved one, and also, polar coordinates are obviously more suitable than rectangular coordinates for circular cross sections. In Fig.4(a), it can be clearly shown that the full cross section area is surrounded by an 8×8 grids, which could evaluate the damage level according to the wave velocity and duration time. However, there are no elements in the 1, 8, 57, 64 grids, which may trigger a high probability of calculation error. The traditional method was improved by drawing a circumcircle and 64 pieces of sectors were divided as Fig.4(b), so that the grid boundary coincides with the cross section which aims to improve the signal to noise ratio (SNR). With the assumption that the velocity of ultrasonic wave is v (x, y) and the duration time of each path ti can be presented as Eq.1. Fig.5 shows the

schematic diagram of a series of tiny grids, meanwhile, the velocity of ultrasonic wave is v (x, y) can be considered as a constant value in this case. Thus, Eq.1 can be rewritten as Eq.2 and the calculation result of Eq.3 emphasizes the result of slowness, which can reveal the internal damages of cross sections. A three-dimensional diagram would be much helpful to evaluate the damage level according to the ultrasonic signals, meanwhile, the denser the mesh, the higher the detection accuracy. The calculation principle is reasonable according to what mentioned above, hence, the key point that matters is the transmission procedure of ultrasonic signals, which can be expressed as Eq.4.

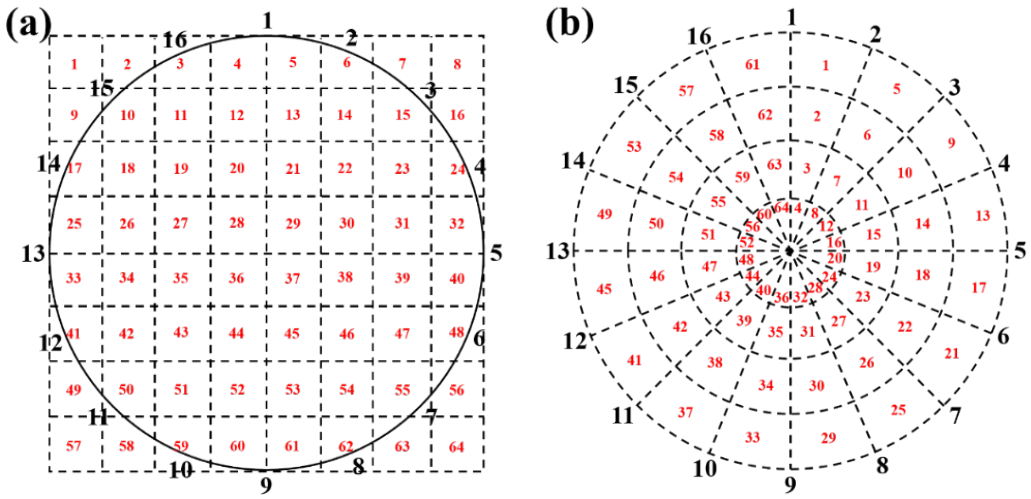

Fig.4 The improvement of mesh generation (a) Traditional one (b) Improved one

$$t_i = \int_{R_i} \frac{1}{v(x,y)} ds \ (i = 1, 2, 3, \dots, n) \tag{1}$$

Where n is the number of ultrasonic paths and Ri is the route of ith ultrasonic path.

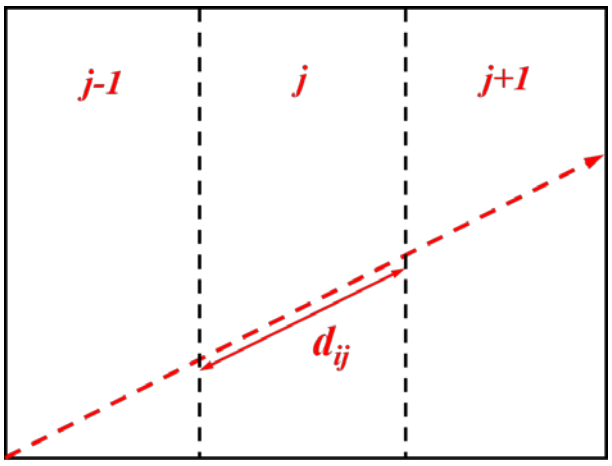

Fig.5 Schematic diagram of tiny grids

$$t_i = \sum_{j=1}^{m} d_{ij}/v_i \ (x, y) \ \ (i = 1, 2, \dots, n; \ j = 1, 2, \dots, m) \tag{2}$$

Where ti is the duration time of ith path and dij is the the length of the ith through the jth grid, n is the number of paths and m is the number of grids.

$$\begin{pmatrix} a_{11} & a_{12} & a_{13} & a_{14} & \dots & a_{1m} \\ a_{21} & a_{22} & a_{23} & a_{24} & \dots & a_{2m} \\ a_{31} & a_{32} & a_{33} & a_{34} & \dots & a_{3m} \\ a_{41} & a_{42} & a_{43} & a_{44} & \dots & a_{4m} \\ \vdots & \vdots & \vdots & \vdots & \vdots & \vdots \\ a_{n1} & a_{n2} & a_{n3} & a_{n4} & \cdots & a_{nm} \end{pmatrix} \begin{pmatrix} S_1 \\ S_2 \\ S_3 \\ S_4 \\ \vdots \\ S_m \end{pmatrix} = \begin{pmatrix} t_1 \\ t_2 \\ t_3 \\ t_4 \\ \vdots \\ t_m \end{pmatrix} \tag{3}$$

Where S=1/v, which is called the slowness of ultrasonic wave.

$$c = \lambda f \tag{4}$$

Where c is the wave velocity of ultrasound (m/s), λ is the wave length (mm) and f is the frequency of ultrasonic wave.

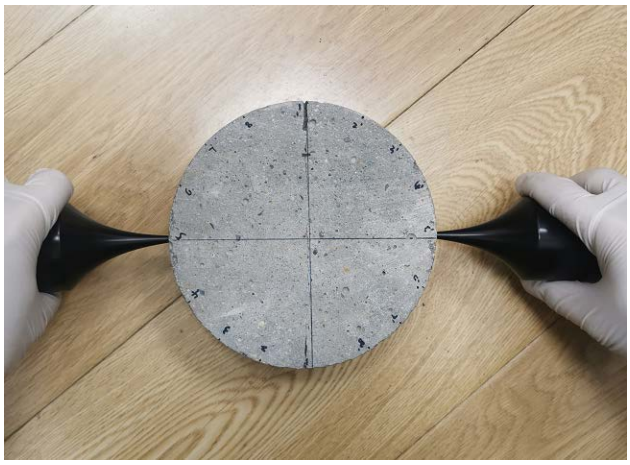

Fig.6 Real diagram of ultrasonic testing

Based on Eq.3, the ultrasonic path distance of every single grid can be calculated by the software AutoCAD, meanwhile, the transmissional duration time were collected corresponding to every single ultrasonic path respectively from the device. After that, the slowness of 64 grids will be calculated based on Eq.3 and software Matlab. It is worth mentioning that Eq.3 will be transferred to Eq.6 in order to obtain the most optimal mathematical solutions, and the boundary condition was set as S>0. Thus, all the solutions are optimized by the CVT optimization module of software Matlab and the optimal solution that meets the boundary conditions is selected. After that, the color cloud maps were drawn based on 64 slowness respectively in polar coordinates by software Matlab and the color difference represents the slowness variation. Afterwards, ultrasonic CT and X-ray CT technologies were adopted to scan the cross-sectional signals along the longitudinal direction every 10 mm of the specimen, which aims to prove the accuracy and reliability of UCT technique. According to the UCT results, the signals of each section is compared with each other to judge the positions and trends of cracks comprehensively, so as to evaluate the safety performance of the whole components.

$$\lim \left| \begin{pmatrix} a_{11} & a_{12} & a_{13} & a_{14} & \dots & a_{1m} \\ a_{21} & a_{22} & a_{23} & a_{24} & \dots & a_{2m} \\ a_{31} & a_{32} & a_{33} & a_{34} & \dots & a_{3m} \\ a_{41} & a_{42} & a_{43} & a_{44} & \dots & a_{4m} \\ \vdots & \vdots & \vdots & \vdots & \vdots & \vdots \\ a_{n1} & a_{n2} & a_{n3} & a_{n4} & \cdots & a_{nm} \end{pmatrix} \begin{pmatrix} S_1 \\ S_2 \\ S_3 \\ S_4 \\ \vdots \\ S_m \end{pmatrix} - \begin{pmatrix} t_1 \\ t_2 \\ t_3 \\ t_4 \\ \vdots \\ t_m \end{pmatrix} \right| = 0 \quad (S > 0) \tag{6}$$

3 Results and Discussion

3.1 Imaging of the Penetration Cracks

Fig.7 presents the comparison of test results between traditional algorithm, improved algorithm and X-ray CT respectively. It can be clearly observed that the significant enhancement is strongly exhibited from the improved algorithm of ultrasonic CT color cloud map. First of all, the highlights caused by shear wave vanished, because the optimized algorithm ensured a certain distance between transmitting and receiving probes, so as to avoid the generation of shear waves, which would influence the experimental results. Secondly, the radial degree of the central region is critically reduced, which is due to the ultrasonic ray arrangement in the improved algorithm is more uniform, so that the attenuation of ultrasonic signal caused by cracks is more evident. Finally, but most importantly, the ultrasonic signals at the damage positions are more prominent and conducive to observation. In Fig.7, the results of X-ray CT also emphasize that ultrasonic CT is capable of reflecting the damage level of cross sections of cement-based materials, while the damage locations observed from UCT have good agreement with that of XCT, which indicates the reliability of UCT technique.

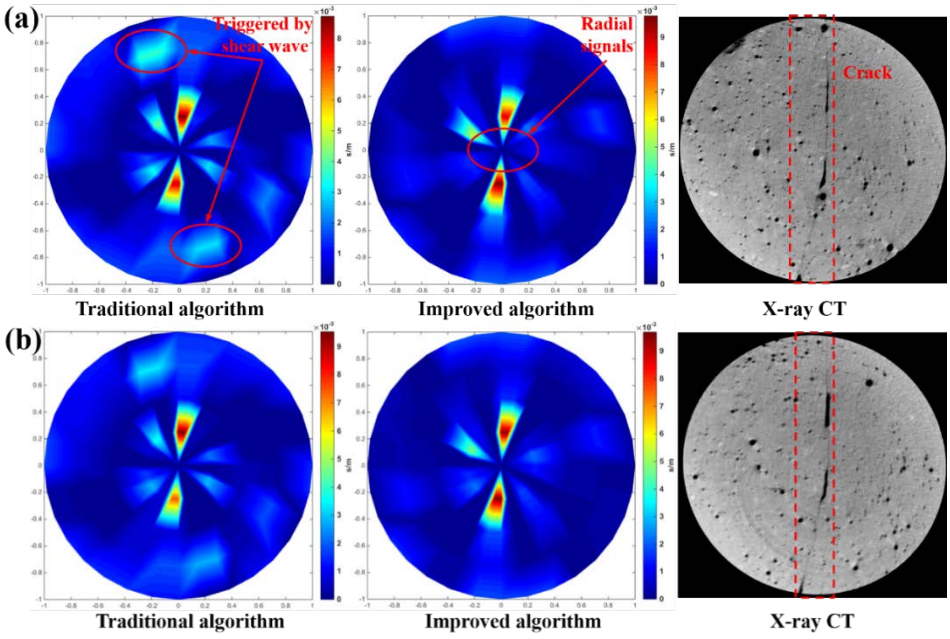

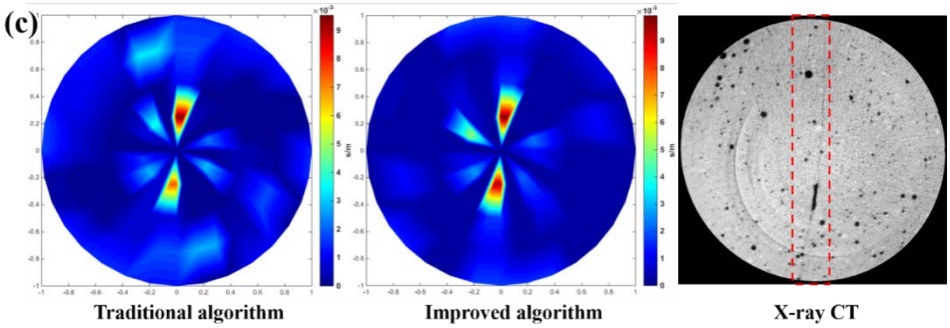

Fig.7 Comparison of CT diagrams between traditional algorithm, improved algorithm and X-ray CT (a) 5 mm (b) 15 mm (c) 25 mm

3.2 Imaging of the Local Damage

Fig.8 presents the CT diagrams along the longitudinal direction of the specimen with a drilled hole while the location can be clearly observed, which has good agreement with its physical location, meanwhile, some influencing signals were produced around the hole, which causes several distractions to the test results. The ultrasonic signals along the longitudinal five cross-sections present a high degree of consistency, which is capable of accurately reflecting the positions of the local damage. Comparing the imaging of the penetration crack with that of the drilled hole (local damage) using the improved algorithm, two totally various types of fractures, which can be easily found that the penetration crack is much more sensitive to the ultrasonic wave than the drilled hole which belongs to the local damage type, even though the scale of the crack is relatively tiny. Unlike the penetration cracks, the color diagram is not radial at the local damage place due to the limited fracture scale, moreover, the signal to noise ratio of the ultrasonic CT method will be much higher with the increasing of the fracture size.

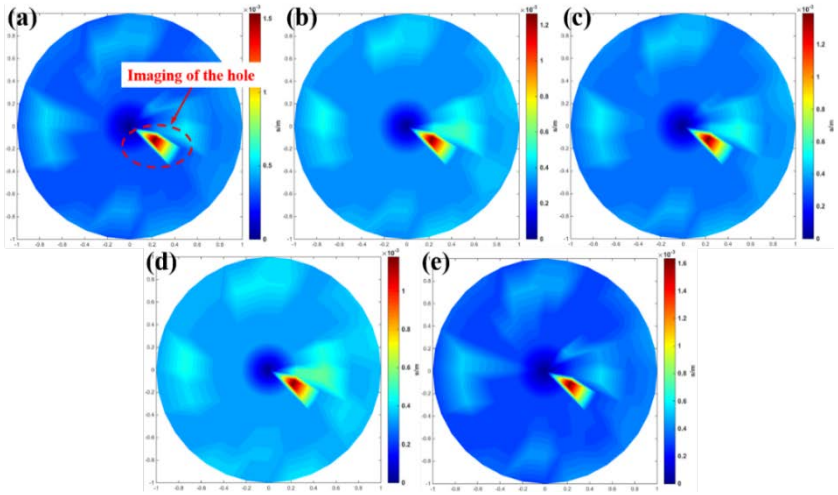

Fig.8 CT diagrams of the specimen with a drilled hole (a) 5 mm (b) 15 mm (c) 25 mm (d) 35 mm

4 Conclusions

In this paper, an improved ultrasonic CT algorithm was proposed and highlighted in order to make up for the drawbacks of traditional CT algorithm, and also, the experiments had been carried out to verify the accuracy and reliability of the enhanced CT algorithm. The conclusions can be drawn as follows.

(1) Ultrasound is a relatively promising approach to detect the internal fractures inside cement-based materials, and also, effective evaluating the internal cracks depends on the detection of the ultrasonic signals attenuation that perpendicular to the internal cracks. Moreover, the local damage is less sensitive to the ultrasonic wave than the penetration crack.

(2) The application of computerized tomography increases the applicability of ultrasonic technique, furthermore, the improved algorithm enhances the accuracy by novel arrangement type of transmitting and receiving ultrasonic probes, which reduces the formation of shear waves.

(3) The precision of the ultrasonic CT technology depends on the accuracy of ultrasonic apparatus and the density of mesh division, in addition, the crack width is still tough to be quantified according to the ultrasonic signals, which still needs to be further studied in a not distant future.

Acknowledgements

This work is a part of a series of projects financially supported by the Chinese National Key Research and Development Program Grant No. 2020YFC1522403.

References

Y. Liu, A.K. Schindler, J.S. Davidson. (2018). *Finite-element modeling and analysis of early-age cracking risk of cast-in-place concrete culverts*, Transportation Research Record Journal of the Transportation Research Board, 27, 24-36.

Y. Yu, Z. Jin, S. Shao, X. Zhang, C. Xiong. (2021). *Evolution of temperature stress and tensile properties of concrete during steam-curing process*, Construction and Building Materials, 305, 124691.

Z. Jin, W. Sun, Y. Zhang, J. Jiang, J. Lai. (2007). *Interaction between sulfate and chloride solution attack of concretes with and without fly ash*, Cement and Concrete Research, 37(8), 1223-1232.

J. Bao, S. Li, Z. Yu, J. Xu, Y. Li, P. Zhang, Z. Si, S. Gao. (2021). *Water transport in recycled aggregate concrete under sustained compressive loading: Experimental investigation and mesoscale numerical modelling*, Journal of Building Engineering, 44, 103373.

D. Hou, J. Yu, P. Wang. (2019). *Molecular dynamics modeling of the structure, dynamics, energetics and mechanical properties of cement-polymer nanocomposite*, Composites Part B: Engineering, 162, 433-444.

X. Wang, J. Liu, Z. Jin, F. Chen, P. Zhong, L. Zhang. (2022). *Real-time strain monitoring of reinforced concrete under the attacks of sulphate and chloride ions based on XCT and DIC methods*, Cement and Concrete Composites, 125, 104314.

L. Li, K. Li. (2015). *Permeability of microcracked solids with random crack networks: Role of connectivity and opening aperture*, Transport in Porous Media, 109(1), 217-237.

N. Li, Z. Jin, G. Long, L. Chen, Q. Fu. (2021). *Impact resistance of steel fiber-reinforced self-compacting concrete (SCC) at high strain rates*, Journal of Building Engineering, 48, 102212.

Z. Li, Z. Jin, P. Wang, T. Zhao. (2021). *Corrosion mechanism of reinforced bars inside concrete and relevant monitoring or detection apparatus: A review*, Construction and Building Materials, 279, 122432.

Z. Li, Z. Jin, Y. Gao, T. Zhao, P. Wang, Z. Li. (2020). *Coupled application of innovative electromagnetic sensors and digital image correlation technique to monitor corrosion process of reinforced bars in concrete*, Cement and Concrete Composites, 113, 103730.

J. Zhang, T. Fan, H. Ma, Z. Li. (2015). *Monitoring setting and hardening of concrete by active acoustic method:*

Effects of water-to-cement ratio and pozzolanic materials, Construction and Building Materials, 88: 118-125.
J. Zhang, H. Ma, W. Yan, Z. Li. (2016). *Defect detection and location in switch rails by acoustic emission and Lamb wave analysis: A feasibility study*, Applied Acoustics, 105, 67-74.
S. Ham, J.S. Popovics. (2015). *Application of contactless ultrasound toward automated inspection of concrete structures*, Automation in Construction, 58, 155-164.
G. Kim, J.-Y. Kim, K.E. Kurtis, L.J. Jacobs. (2017). *Drying shrinkage in concrete assessed by nonlinear ultrasound*, Cement and Concrete Research, 92, 16-20.
A. Quiviger, C. Payan, J.F. Chaix, V. Garnier, J. Salin. (2012). *Effect of the presence and size of a real macro-crack on diffuse ultrasound in concrete*, NDT&E International, 45(1), 128-132.
E. Ahn, M. Shin, J.S. Popovics, R.L. Weaverc. (2019). *Effectiveness of diffuse ultrasound for evaluation of micro-cracking damage in concrete*, Cement and Concrete Research, 105862.